Robust adaptive speed control of uncertain hybrid electric vehicle using electronic throttle control with varying road grade

Article *in* Nonlinear Dynamics · April 2013

DOI: 10.1007/s11071-013-1128-9

CITATIONS
46

READS
555

2 authors:

Anil Kumar Yadav
Dr. B. R. Ambedkar NIT Jalandhar
76 PUBLICATIONS **1,416** CITATIONS
SEE PROFILE

Prerna Gaur
Netaji Subhas University of Technology
132 PUBLICATIONS **1,492** CITATIONS
SEE PROFILE

Nonlinear Dyn (2014) 76:305–321
DOI 10.1007/s11071-013-1128-9

ORIGINAL PAPER

Robust adaptive speed control of uncertain hybrid electric vehicle using electronic throttle control with varying road grade

Anil Kumar Yadav · Prerna Gaur

Received: 25 February 2013 / Accepted: 21 October 2013 / Published online: 12 November 2013

Abstract The design objective of this paper is to apply various control techniques to control the speed of a hybrid electric vehicle (HEV) using an electronic throttle control system (ETCS). The DC servo motor is used for controlling the angular position of the throttle valve. A proportional-integral-derivative (PID), a self-tuning fuzzy PID (STF-PID) controller and a model reference adaptive system (MRAS) with a sliding mode (SM) adaptation mechanism are used for controlling the speed of the nonlinear vehicle. The integral error performance indices (IEPI) such as the integral of the absolute error (IAE), the integral of the square of error (ISE) and the time domain performance specifications such as overshoot (OS), settling time (ST) and rise time (RT) are taken into consideration for the performance analysis of HEV. The robust H_∞ controller using mixed sensitivity approach is designed and implemented for the linearized HEV. The robust stability of uncertain HEV with H_∞ controller using Kharitonov's theorem is analyzed, and the stability margin of the linearized vehicle system is determined. These control techniques are developed to achieve the robust performance of the throttle controlled HEV with the target to achieve a wide range of speed, fuel economy, reduced pollution and improved efficiency.

Keywords Adaptive control · Electronic throttle control system · H_∞ control · HEV · Robustness · Stability margin

A.K. Yadav (✉) · P. Gaur
Division of Instrumentation and Control Engineering,
Nataji Subhas Institute of Technology, Dwarka,
New Delhi, India
e-mail: anilei007@gmail.com

1 Introduction

In recent years, increasing concern for environment and economy has made the use of a hybrid electric vehicle (HEV) indispensable and ubiquitous in nature. The limitation of a pure electric vehicle (EV) is related to the variation in vehicle speed with large variation in road grade or slope. The EV must be converted into HEV which is powered by a conventional internal combustion engine (ICE) or an electric motor along with a battery or both, depending on the factors such as speed, required power, and amount of charge left in the batteries, i.e., state of charge, etc. The emitted pollutants like carbon monoxide, hydrocarbon and nitrogen oxide are strongly dependent on the air–fuel ratio. These emissions are a major source of pollution that causes the greenhouse effect which in turn leads to global warming. Furthermore, electric power used for the battery of EVs can also be generated using nonconventional sources like solar and wind, etc., which are environment friendly [1–5].

Energy management and optimal power flow in a plug-in HEV with vehicle dynamics is discussed in the

literature review [6–9], but the plug-in HEV fails under large speed variation such as in a terrain region, i.e., when the road slope is unpredictable, and fuel stations are less abundant. There are many countries and places where the implementation of a constant speed vehicle, i.e., controlling pure EV is more difficult. In the entire vehicle such as a conventional vehicle, series, parallel, and HEV, etc., ICE plays a key role for better and wider speed performance. ICEs are used in almost all vehicles in all fields such as heavy trucks, military trucks, tractors, ambulances, trains, aircrafts, etc., which are a major source of pollution, high fuel consumption, poor speed performance, and less efficiency at low speed. These variables depend on the throttle position which is controlled by a high performance DC servo motor as proposed in this paper. Controlling the throttle position using electric motor drives is called an electronic throttle control system (ETCS). With the HEV and ETCS, a wide range of vehicle speed with varying road grade may be achieved. This may also control the pollutant emission and improve fuel economy and efficiency. The throttle is used as a valve to regulate the air mass flow into the engine combustion system [5, 10].

The HEV with ETCS and nonlinear vehicle dynamics make a nonlinear and unstable system. The linear control techniques cannot handle this problem due to high nonlinearities in the system. Several strategies such as PID, optimal linear quadratic regulator (LQR), self-organizing control and fuzzy logic controller (FLC), etc. have been used for speed control of a linearized vehicle model with fixed road grade using throttle position control in [4]. Many nonlinear control techniques such as sliding mode, model predictive control [8], adaptive control like MRAS [11, 12], self-tuning fuzzy PID control [19], self-organizing fuzzy logic control [18], fuzzy logic control, and neural network based control [12] effectively handling nonlinearities and the uncertainty problem are discussed in [11–19]. The adaptive vehicle speed control with input injections is discussed in [20]. The self-tuning fuzzy logic PID controller designed to tune the gain of K_p, K_i and K_d of the PID controller is used in this paper. The integral error performance indices (IEPI) such as the integral of the absolute error (IAE) and the integral of the square of the error (ISE) are used as measures of the HEV performance. The time domain performance parameters such as the overshoot (OS), settling time (ST) and rise time (RT) are also studied to get better all-round performance of HEV. Among all the adaptive control techniques, MRAS schemes are the most common strategies employed due to their relative simplicity and low computational effort [11, 12]. In this paper, a self-tuning fuzzy PID controller (STF-PID) and MRAS with sliding mode adaptation mechanisms in a cascade structure are proposed. In this cascade structure, there are two loops, inner and outer. In this paper, a proportional-integral (PI) controller is used in the inner loop, and PID, STF-PID controller and MRAS are applied in the outer loop. In MRAS, the dominant poles (DP) based reference models are designed and the performance parameters like ST, RT, OS, and the steady state error (E_{ss}) are also taken into consideration. The main advantage of MRAS over STF-PID is it has a reference model (RM) which gives the desired performance of the system. This motivates the authors to find the desired trajectory, i.e., desired speed that is automatically achieved by using a suitable placement of dominant poles of RM [13].

In practical control systems, at least two types of uncertainties, namely unstructured and structured or parametric uncertainties, are present. The parametric uncertainty represents the lack of precise knowledge of the actual system parameters [21]. In this paper, the focus is on the parametric uncertainties because vehicle parameters used in modeling are varying within a prespecified range. For the analysis of parametric uncertainties, Kharitonov's theorem and H_∞ controller using mixed sensitivity approach are proposed for the linearized system. Generally, H_∞ controller deals with the unstructured uncertainties, but in this paper it is proposed for the system having structured uncertainties. In 1978, the Russian mathematician Kharitonov published a paper in a mathematical journal which is now used for problems of robust control [22]. The applications of Kharitonov's theorem in various fields are given in [23, 24], and may also be used in other similar applications such as the control of an induction motor drive, control of aircraft, etc. The H_∞ control design technique, however, directly address the problem of robustness by deriving controllers which maintain system response and error signals to within prescribed tolerances, despite the presence of noise in the system [25, 26]. A design methodology of weighting functions has been proposed for the H_∞ mixed sensitivity problem in [27, 28].

In this paper, the H_∞ control theory is used for the design of the controller, while Kharitonov's theorem

is used for robust stability analysis of HEV with parametric uncertainty. The stability margin of the uncertain HEV with reduced H_∞ controller is determined using Kharitonov's theorem. The order reduction of the H_∞ controller is achieved by using Routh's order reduction technique [30, 31]. For a better performance analysis of a system, it is required to have proper balance in the time domain, frequency domain and IEPI. All the above mentioned performance specifications are considered in this paper.

2 Problem formulation and modeling

The architecture of HEV considered in this paper is given in Fig. 1(a) [6] and the mechatronic system of an engine with ETCS is shown in Fig. 1(b). It may be called the single mode power split series/ parallel or combined. The planetary gear set creates both series and parallel paths for power flow to the wheels. The parallel flow paths (dashed arrows) include a path from the engine to the wheels and a path from the battery, through the motors, to the wheels. On the other hand, the series flow path takes power from the engine to the battery first, and then back through the electrical system to the wheels (solid arrows). This configuration has many features such as a wide range of speed, improves the overall efficiency, reduces pollution; it may also be used in military vehicles, unmanned vehicles in robotics, bomb blasting and bomb diffusion process, etc. The planetary gear set may have an electronic switch, programmed according to the road grade, desired vehicle speed and state of charge of the battery. It is clear from Fig. 1(a) that the engine plays a key role in all the configurations of the vehicle and the power at the initial, i.e., transient state. Hence it is necessary to control the engine speed which varies with time and strongly depends on fuel power, i.e., air–fuel ratio. The air–fuel ratio is responsible for the pollutant emission, power required by the vehicle, efficiency of the vehicle, etc.

The numerical values of uncertain HEV in SI units used for simulation and robustness analysis are given in Table 1. In Fig. 1(b), the ETCS uses a DC servo motor to rotate the throttle plate. Here the DC servo motor is controlled by the applied motor voltage E_a [10]:

$$\frac{di_a}{dt} = \left(\frac{1}{L_a}\right)\left(-R_a i_a - K_b \frac{d\theta_m}{dt} + E_a\right) \tag{1}$$

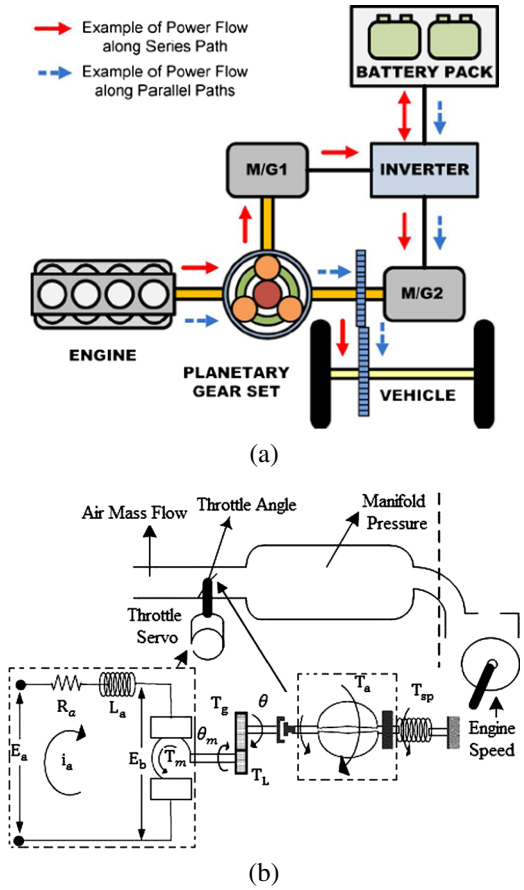

Fig. 1 (**a**) Architecture of HEV. (**b**) Mechatronic system of an engine with ETCS

where i_a is armature current (A), θ_m is armature angular position (rad). The back EMF E_b due to the motor rotation is $K_b \cdot d\theta_m/dt$. The meaning of symbols used in equations is given in Table 1.

The motor and rotational dynamics of the throttle are given by

$$\frac{d^2\theta_m}{dt^2} = \left(\frac{1}{J_m}\right)\left(-B_m\left(\frac{d\theta_m}{dt}\right) - T_L + T_m\right), \tag{2}$$

$$\frac{d^2\theta}{dt^2} = \left(\frac{1}{J_g}\right)\left(-T_{sp} - B_t\left(\frac{d\theta}{dt}\right) - T_a + T_g\right) \tag{3}$$

where the gear ratio is N, the engine speed is defined as $N = \theta_m/\theta = T_g/T_L$, T_a is the torque due to airflow (N m), T_g is the torque transmitted from gears (N m), T_L is the load torque (N m), T_m is the torque applied by motor (N m), T_{sp} is the return spring torque (N m),

Table 1 Numerical values and parametric uncertainty of HEV

Descriptions	Symbol	Value (SI unit)	Uncertainty
Armature resistance	R_a	2 Ω	[1.5, 2.5]
Armature inductance	L_a	0.003 H	[0.002, 0.004]
Back EMF constant	K_b	0.11 V s/rad	[0.07, 0.15]
Gear ratio	N	4	[2, 6]
Motor torque constant	K_t	0.1 N m/A	[0.08, 0.12]
Throttle spring constant	K_{sp}	0.4 N m/rad	[0.3, 0.5]
Focal point of airflow on plate	R_{af}	0.002 m	[0.001, 0.003]
Pre-tension angle of spring	θ_0	$\pi/2$ rad	–
Throttle plate radius	R_p	0.0015 m	[0.001, 0.002]
Motor damping constant	B_m	0.03 N ms/rad	[0.02, 0.04]
Throttle damping constant	B_t	0.002 N ms/rad	[0.001, 0.003]
Motor inertia	J_m	0.001 kg m^2	[0.0008, 0.0012]
Throttle inertia	J_g	0.005 kg m^2	[0.003, 0.007]
Equivalent inertia	J	0.021 kg m^2	[0.009, 0.0502]
Damping constant	B	0.482 N ms/rad	[0.082, 1.443]
Vehicle mass	m	1000 kg	[750, 1250]
Drag coefficient	α	0.48 N/(m/s)^2	[0.4, 0.56]
Engine force coefficient	γ	12500 N	[10000, 15000]
Engine idle force	F_i	6400 N	[5500, 7300]
Engine time constant	τ_e	0.5 s	[0.2, 0.8]
Bearing damping coefficient	b_w	0.035 N ms/rad	[0.03, 0.04]
Radius of tire	r_{tire}	70 mm	[50, 90]
Friction coefficient	μ	0.011	[0.01, 0.012]
Gravity acceleration	g	9.8 m/s^2	–
Road slope/grade	β	Variable	[±2°, ±30°]
Desired values	$*$		

θ is the throttle plate angular position in radians. The motor torque T_m is defined as

$$T_m = K_t i_a. \tag{4}$$

From Eqs. (1)–(4), we have

$$\frac{di_a}{dt} = \left(\frac{1}{L_a}\right)\left(-R_a i_a - K_b N \frac{d\theta}{dt} + e_a\right), \tag{5}$$

$$\frac{d^2\theta}{dt^2} = \left(\frac{1}{J}\right)\left(-B\left(\frac{d\theta}{dt}\right) + NT_m - T_{sp} - T_a\right) \tag{6}$$

where $J = N^2 J_m + J_g$ and $B = N^2 B_m + B_t$.

A stiff rotational spring returns the plate to a closed position when E_a is zero. The spring assembly has been initialized to an angle θ_0 which produces a closing torque. The spring torque T_{sp} may be described as

$$T_{sp} = K_{sp}(\theta + \theta_0). \tag{7}$$

The airflow over the throttle plate induces a small torque T_a given by

$$T_a = R_{af} F_a \cos\theta. \tag{8}$$

The variable F_a denotes the air force acting on the plate parallel to the air flow direction:

$$F_a = \Delta P A_p \cos\theta \tag{9}$$

where $\Delta P = P_{\text{atm}} - P_m$, the throttle plate area (m^2) is $A_p = \pi R_p^2$ and $P_m = f(\theta, P_{\text{atm}}, N)$. The manifold pressure P_m is a nonlinear throttle angle dependent function that approaches the atmospheric pressure (P_{atm}) as the throttle approaches a wide-open state. Hence (8) can be written as

$$T_a = R_{af} \Delta P \pi R_p^2 \cos^2\theta. \tag{10}$$

Equations (5) to (10) give the nonlinear mathematical model of ETCS.

For the simplification and representation of system in the s-domain, taking the Laplace transform of (5) and (6), we obtain

$$L_a s I_a(s) = -R_a I_a(s) - K_b N s\theta(s) + E_a(s)$$
$$\Rightarrow \quad I_a(s) = \frac{E_a(s) - K_b N s\theta(s)}{sL_a + R_a}, \tag{11}$$
$$Js^2\theta(s) = -Bs\theta(s) + NK_t I_a(s) - T_{sp} - T_a. \tag{12}$$

From (11) and (12),

$$Js^2\theta(s) = -Bs\theta(s) + NK_t\left(\frac{E_a(s) - K_b N s\theta(s)}{sL_a + R_a}\right) - T_{sp} - T_a. \tag{13}$$

For simplicity, consider the throttle to be at the open state, i.e., $\theta = \pi/2$, which is equal to θ_0 as given in Table 1. Hence

$$T_a = 0 \quad \text{and} \quad T_{sp} = K_{sp} \times 2 \times \theta(s). \tag{14}$$

From (13) and (14),

$$\left[L_a Js^3 + R_a Js^2 + BL_a s^2 + R_a Bs + N^2 K_t K_b + 2K_{sp} L_a s + 2K_{sp} R_a\right]\theta(s) = NK_t E_a(s) \tag{15}$$

$$\frac{\theta(s)}{E_a(s)} = \frac{NK_t/L_a J}{s^3 + \frac{R_a J + BL_a}{L_a J}s^2 + \frac{R_a B + N^2 K_t K_b + 2K_{sp} L_a}{L_a J}s + \frac{2K_{sp} R_a}{L_a J}}. \tag{16}$$

From Table 1, putting the nominal values in (16), we get the transfer function of ETCS:

$$\frac{\theta(s)}{E_a(s)} = \frac{6349}{s^3 + 689.7s^2 + 1.82 \cdot 10^4 s + 2.54 \cdot 10^4}. \tag{17}$$

The explicit dynamics of the nonlinear vehicle [4, 6] is given as follows;

$$m\frac{dV}{dt} = F_e(\theta) - F_{\text{wheel}} - F_g, \tag{18}$$
$$\tau_e \frac{dF_e(\theta)}{dt} = -F_e(\theta) + F_{e1}(\theta) \tag{19}$$

where

$$F_{e1}(\theta) = F_i + \gamma\sqrt{\theta}. \tag{20}$$

F_e is the engine force that is a function of the throttle position, θ is the angular throttle position, V is the vehicle speed, F_g is the gravity induced force, which is a function of the road grade or road slope β. The road slope may be positive or negative. As a disturbance, it is considered a non-deterministic variable and represented as

$$F_g = m \cdot g \cdot \sin\beta. \tag{21}$$

F_{wheel} is a force acting on the wheel, in the literature [6] it is given as F_{road} which is

$$F_{\text{wheel}} = F_{\text{roll}} + F_{\text{drag}} + F_{\text{damp}}, \tag{22}$$
$$F_{\text{roll}} = \mu \cdot m \cdot g \cdot \cos\beta, \tag{23}$$
$$F_{\text{drag}} = 0.5 \times \rho \times A_{fr} \times c_d \times V^2 = \alpha V^2 \tag{24}$$

where ρ, A_{fr} and c_d represent the density of air (kg/m^3), the vehicle effective frontal area (m^2), and the aerodynamic drag coefficient (N s^2/kg m), respectively.

$$F_{\text{damp}} = \frac{b_w \cdot V}{r_{\text{tire}}} \tag{25}$$

where b_w is the bearing's damping coefficient and r_{tire} is an effective vehicle tire radius. Note that this expression for the wheel damping, as well as other derivations, assumes a direct proportionality between the wheel angular velocity and vehicle speed. After combining (18)–(25), we get

$$m\frac{dV}{dt} = F_i + \gamma\sqrt{\theta} - \tau_e\frac{dF_e(\theta)}{dt} - \mu \cdot m \cdot g \cdot \cos\beta - \alpha V^2 - \frac{b_w \cdot V}{r_{\text{tire}}} - m \cdot g \cdot \sin\beta. \tag{26}$$

The complete mathematical model of the nonlinear vehicle considered in this paper is given by (26). Using (26), the Simulink model of the nonlinear vehicle is designed which is given in Fig. 2. In Fig. 2, $\beta = 10^\circ$ (0.175 radian) is considered for the simplification of the vehicle model, but during simulation β is taken as a random value with variance of $\pi/10$ radian, which gives a non-deterministic slope of the road.

The MATLAB command 'linmod' is used for the linearization of the nonlinear model in [29] and here the same command is used for the linearization of the nonlinear vehicle, hence the transfer function of the vehicle is

$$\frac{V(s)}{\theta(s)} = \frac{7906}{s^2 + 2s + 0.001}. \tag{27}$$

After combining (17) and (27), the overall transfer function $G_N(s)$ of the system with nominal values is given in (28):

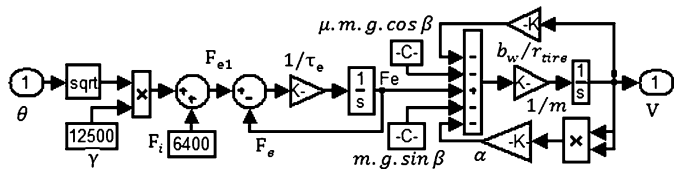

Fig. 2 Simulink model of the nonlinear vehicle

$$\frac{V(s)}{E_a(s)} = \frac{5\times 10^7}{s^5+691.7s^4+1.95\cdot 10^4 s^3+6.17\times 10^4 s^2+5.08\cdot 10^4 s+25.4}. \quad (28)$$

Equation (29) and (30) represent the transfer function of the system for lower and upper limit values, respectively, that are given in Table 1 and are required for robustness analysis of the overall vehicle model under parametric uncertainty;

$$G_L(s) = \frac{1.87\times 10^8}{s^5+764s^4+1.19\cdot 10^4 s^3+9.1\times 10^4 s^2+2.5\cdot 10^5 s+200}, \quad (29)$$

$$G_U(s) = \frac{1.7\times 10^7}{s^5+655s^4+2.2\cdot 10^4 s^3+3.9\times 10^4 s^2+1.56\cdot 10^4 s+5.5}. \quad (30)$$

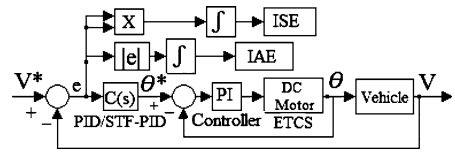

Fig. 3 Proposed control block diagram of the complete system with the controller

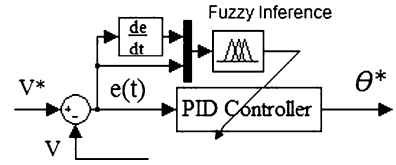

Fig. 4 Structure of self-tuning fuzzy PID controller

3 Self-tuning fuzzy PID controller

The conventional tuning of a PID controller like Ziegler Nichols doesn't apply for all nonlinear, uncertain and time varying systems. Hence the PID controller tuned by the hand tuning rule [4] and fuzzy logic is used here, and this may be called a self-tuning fuzzy PID controller; it may also be called adaptive control because the controller adapts to the non-deterministic variation of the road grade or slope, it also gives robust performance which is verified by lower and upper limit values as given in Table 1. The transfer function of the generalized PID controller is given in [4], namely

$$C(s) = K_P + \frac{K_i}{s} + K_d s = K_P\left(1+\frac{1}{T_i s}+T_d s\right) \quad (31)$$

where K_p, K_i, and K_d are proportional, integral and derivative gains, respectively. T_i is the reset time which is equal to K_p/K_i, and T_d is the rate time which is equal to K_d/K_P. The proposed control block diagram of the complete system with the controller is represented in Fig. 3.

In the STF-PID controller, the parameters of the PID controller, K_p, K_i and K_d, are tuned by fuzzy logic [19]. The gains of the PID controller are not often properly tuned for the nonlinear vehicle with unpredictable parameter variations like road slope, and manual tuning or hand tuning rule takes a lot of time. Hence, it is necessary to automatically tune the PID controller parameters. The structure of the self-tuning fuzzy PID controller is shown in Fig. 4. For the design and implementation of the STF-PID controller, there are two inputs to fuzzy inference, error $e(t)$ and derivative of error $de(t)$, and three outputs, K'_p, K'_i and K'_d. In this controller, the designing processes of the rules are based on the properties of the PID controller and the characteristic of the HEV.

Assume that the variable ranges of the PID controller parameters K_p, K_i, K_d are $[K_{p\min}, K_{p\max}]$, $[K_{i\min} K_{i\max}]$, $[K_{d\min}, K_{d\max}]$, respectively. The range of each parameter is determined by using simulation results of the PID controller. Consider the range of the PID controller parameters K_p, K_i and K_d as [0.1, 10]. These are calibrated as follows:

$$K_p' = \frac{K_p - K_{p\min}}{K_{p\max} - K_{p\min}} = \frac{K_p - 0.1}{10 - 0.1},$$
$$K_i' = \frac{K_i - K_{i\min}}{K_{i\max} - K_{i\min}} = \frac{K_i - 0.1}{10 - 0.1} \quad \text{and} \tag{32}$$
$$K_d' = \frac{K_d - K_{d\min}}{K_{d\max} - K_{d\min}} = \frac{K_d - 0.1}{10 - 0.1}.$$

After simplification of (32), we get

$$K_p = 9.9K_p' + 0.1, \qquad K_i = 9.9K_i' + 0.1 \quad \text{and} \tag{33}$$
$$K_d = 9.9K_d' + 0.1.$$

The linguistic variable levels are assigned as negative big (NB), negative small (NS), zero (ZE), positive small (PS), and positive big (PB). The ranges of these inputs are taken between −0.1 and 0.1, and the membership functions of the outputs K_p', K_i' and K_d' are taken to be triangular. The linguistic levels of the outputs are assigned as small (S), medium small (MS), medium (M), medium big (MB), and big (B), where the ranges are from 0 to 1. The fuzzy rules are as shown in Table 2.

4 MRAS speed observer

The MRAS speed observer consists mainly of an RM, plant and an adaptation mechanism. The adaptation mechanism consists of an adjustable control law and an adjusting mechanism of the control law. In the MRAS, the adjustable control law adjusts in such a way that it minimizes the adaptation error and forces the system to asymptotically stabilize. The second order RM in the form of a differential equation is given as

$$\ddot{y_m} = -2\xi\omega_n \dot{y_m} - \omega_n^2 y_m + \omega_n^2 r. \tag{34}$$

The parameters for RM are the reference value r or set value SV, damping ratio ξ and the natural frequency ω_n that require proper balance in the time domain specifications such as ST, OS, E_{ss}, and RT. In this paper, two RMs are taken for comparative study. The RMs and their performance specifications are given in Table 3. RM-1 with $\xi = 0.7$ gives 4.8 % OS, and RM-2 with $\xi = 1$ gives 0 % OS but other performance parameters such as RT, OS and ST are poor in comparison with RM-1, which is clearly seen in Table 3.

The sliding mode control (SMC) is a variable structure control with high frequency discontinuous control action that switches between several functions depending on the system states. It is one of the most effective and robust nonlinear control techniques [17] of nonlinear vehicles. The principle of SMC is to define a switching control law to drive the nonlinear state trajectory onto a switching surface and maintain this trajectory sliding on this surface for all subsequent time [17]. The control law is based on Lyapunov theory to guarantee the motion of the state trajectory towards the sliding surface. This is done by choosing a hitting control gain to maintain the derivative of the Lyapunov function which is always negative definite [11]. The linearized system which is a fifth order system as given in (28) is used for the observer design, and the nonlinear system as given in (26) is used in simulation. Hence the generalized fifth order system is in the form of a differential equation and written as

$$p^5 y = -a_4 p^4 y - a_3 p^3 y - a_2 p^2 y - a_1 p y - a_0 y + k_1 u \tag{35}$$

where the constants a_4 to a_0 are responsible for the location of poles, k_1 is the gain, u is the control input to the plant and p is a differential operator. The adaptation error is defined as

$$y_e(t) = y_m(t) - y(t) \tag{36}$$

Table 2 Rule base matrix for STF-PID

e	ce				
	NB	NS	ZE	PS	PB
NB	S	S	MS	MS	M
NS	S	MS	MS	M	MB
ZE	MS	MS	M	MB	MB
PS	MS	M	MB	MB	B
PB	M	MB	MB	B	B

Table 3 Dominant pole (DP) based RMs and their performances

Reference model	ξ	ω_n	DP	ST (s)	OS %	E_{SS}		RT (s)
						Step	Ramp	
RM-1 = $\frac{4}{p^2+2.8p+4}$	0.7	2	$-1.4 \pm 1.428j$	2.86	4.6	0.0	0.7	1.1
RM-2 = $\frac{4}{p^2+4p+4}$	1	2	$-2, -2$	2.92	0.0	0.0	1	1.68

where $y(t)$ is the plant output, $y_m(t)$ is the RM output. Choose a sliding surfaces as in [11], namely

$$s = y_e + \int k \cdot y_e \cdot dt, \quad k > 0. \tag{37}$$

Then the error dynamics at the sliding surface $s = 0$ will be forced to decay exponentially to zero. When the system reaches the sliding surface, this gives

$$\dot{s} = \dot{y_e} + k y_e = 0. \tag{38}$$

The error dynamics can be described by

$$\dot{y_e} = -k y_e. \tag{39}$$

The SMC law can be found by using Lyapunov theory and defining the Lyapunov function as

$$v = \frac{1}{2} s^2. \tag{40}$$

According to Lyapunov theory, if the derivative of v is negative definite, this will ensure that the state trajectory will be driven and attracted toward the sliding surface s, and having reached it; it will remain sliding on it until the origin is reached asymptotically [11]. The time derivative of the Lyapunov function in (40) can be calculated as

$$\dot{v} = s\dot{s} = s(\dot{y_e} + k y_e). \tag{41}$$

Putting (34) and (35) into (36) and differentiating (36) yields

$$\dot{y_e} = -2\xi\omega_n y_m - \frac{\omega_n^2 y_m}{p} + \frac{\omega_n^2 r}{p} + a_4 y + \frac{a_3 y}{p} + \frac{a_2 y}{p^2} + \frac{a_1 y}{p^3} + \frac{a_0 y}{p^4} - \frac{k_1 u}{p^4}. \tag{42}$$

If

$$f_1 = -2\xi\omega_n y_m - \frac{\omega_n^2 y_m}{p} + \frac{\omega_n^2 r}{p} + a_4 y + \frac{a_3 y}{p} + \frac{a_2 y}{p^2} + \frac{a_1 y}{p^3} + \frac{a_0 y}{p^4} \quad \text{and} \tag{43}$$

$$f_2 = \frac{k_1}{p^4} \quad \text{then} \quad \dot{y_e} = f_1 - u f_2.$$

From (38) and (43)

$$\dot{s} = f_1 + k \cdot y_e - u f_2. \tag{44}$$

Hence (41) can be written as

$$\dot{v} = s(f_1 + k y_e - u f_2). \tag{45}$$

This derivative is negative definite if

$$(f_1 + k y_e - u f_2) \begin{Bmatrix} <0 & \text{for } s > 0 \\ =0 & \text{for } s = 0 \\ >0 & \text{for } s < 0 \end{Bmatrix}. \tag{46}$$

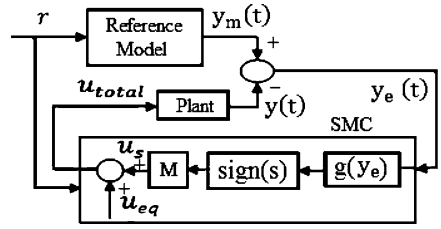

Fig. 5 MRAS speed observer with sliding mode adaptation mechanism

This can be insured if

$$u = \frac{f_1 + k y_e}{f_2} + M \,\text{sign}(s), \quad M > 0 \tag{47}$$

where the sign function is defined as

$$\text{sign}(s) = \begin{Bmatrix} -1 & \text{if } s < 0 \\ +1 & \text{if } s > 0 \end{Bmatrix}. \tag{48}$$

The total control law of the SM adaptation mechanism is represented by (47) and could be written in a general form as

$$u_{\text{total}} = u_{\text{eq}} + u_s \tag{49}$$

where u_{eq} is the equivalent control that defines the control action that keeps the state trajectory on the sliding surface, u_s is the switching control that depends on the sign of the switching surface, and M is the hitting control gain that makes (41) negative definite [11]. The expressions for the equivalent and the switching control functions can be written as

$$u_{\text{eq}} = \frac{f_1 + k y_e}{f_2}, \tag{50}$$

$$u_s = M \,\text{sign}(s), \quad M > 0. \tag{51}$$

The presence of the function f_2 in the denominator of the equivalent control u_{eq} may cause problems in the control and estimation performance of the proposed scheme if its value approaches zero. This problem can be avoided by considering only the numerical values of f_2. The use of the sign function in the SMC in (47) causes high-frequency chattering due to the discontinuous control action that represents a severe problem when the system state is close to the sliding surface [11]. The block diagram of the MRAS observer employing the SM adaptation mechanism is shown in Fig. 5.

5 Robust control

This section presents the robust stability analysis of the linearized HEV with parametric uncertainty using the proportional controller (PC) and Kharitonov's theorem. The gain of PC is derived using the root locus method and H_∞ control theory with an order reduction technique [30, 31].

5.1 H_∞ control theory [25–28]

The standard H_∞ control configuration with weighting functions and proposed speed tracking and robustness analysis control block are given in Fig. 6(a) and 6(b), respectively. The design objective of $C(s)$ is to get both the desired tracing performance and robustness in the predefined range of system parameters which is given in Table 1.

In Fig. 6(a), $G(s)$ is the nominal plant; z, y, SV, and u are the controlled output, the measured output, the exogenous input or set value, and the control input, respectively. They are used to design an H_∞ controller $C(s)$ to get both the desired speed tracking performance and robustness of the system within specified parametric uncertainty. The weighing functions W_1, W_2 and W_3 are as follows: W_1 is the weight for tracking error performance, W_2 is the weight to the controller transfer function, and W_3 is the weight to robust output performance [28]. Figure 6(b) is used for the analysis of the desired speed tracking performance and robustness, i.e., robust stability analysis of the uncertain system. The weighting functions are then selected to keep the parametric uncertainty of the system under prescribed limits as given in Table 1. The H_∞ controller designed using the mixed-sensitivity approach is proposed. The robust control problem consists in stabilizing controller $C(s)$ so that the H_∞ norm of the sensitivity matrix $\|S(j\omega)\|_\infty$ is minimized at the output. This is practically achieved by defining a frequency weighting matrix, $W(j\omega)$. The good tracking performance to a changing desired output requires maximizing the smallest singular value of the complementary sensitivity matrix, $T(s) = 1 - S(s)$. The different frequency ranges for the various optimizations can be specified as three different frequency weighting matrices, $W_1(j\omega)$, $W_2(j\omega)$ and $W_3(j\omega)$, and such

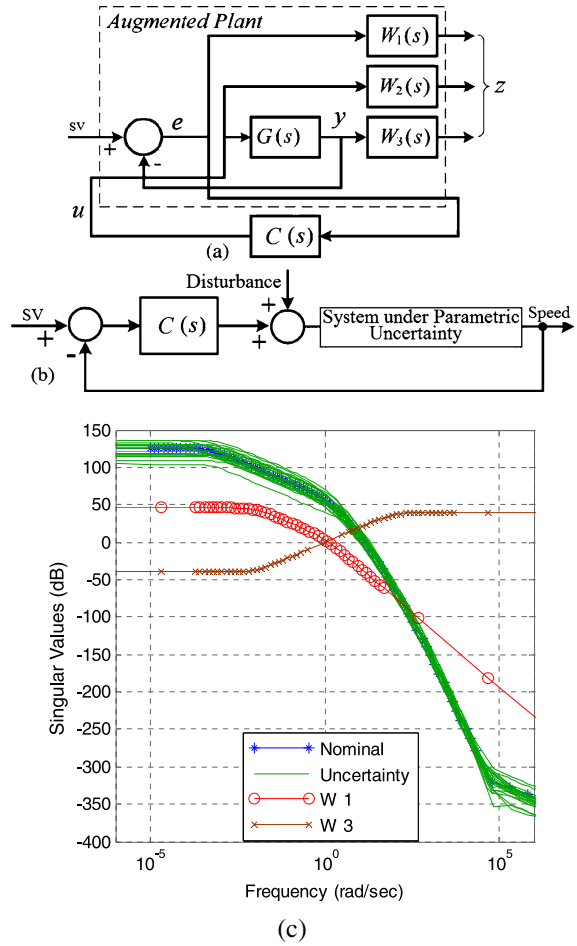

Fig. 6 (**a**) Standard H_∞ control configuration with weighting functions W_1, W_2, W_3, (**b**) Proposed speed tracking and robustness analysis control block. (**c**) Singular values of nominal, plant uncertainty and weighting functions W_1 and W_3

that the H_∞ norm of the mixed-sensitivity matrix, $\|M(j\omega)\|_\infty$, is minimized where

$$M(j\omega) = \begin{bmatrix} W_1(j\omega)S(j\omega) \\ W_2(j\omega)C(j\omega)S(j\omega) \\ W_3(j\omega)T(j\omega) \end{bmatrix}. \tag{52}$$

Formulating the H_∞ optimal control problem in this fashion ensures the specification of both performance and robustness of the desired closed loop system by the three frequency weighting matrices, such that

$$\begin{aligned} &\sigma_{\max}\big(S(j\omega)\big) \le \sigma_{\max}\big(W_1^{-1}(j\omega)\big), \\ &\sigma_{\max}\big(C(j\omega)S(j\omega)\big) \le \sigma_{\max}\big(W_2^{-1}(j\omega)\big), \\ &\sigma_{\max}\big(T(j\omega)\big) \le \sigma_{\max}\big(W_3^{-1}(j\omega)\big) \end{aligned} \tag{53}$$

where $\sigma_{\max}$ represents maximum singular values. The advantages of an H_∞ controller lie in its automatic loop shaping as a function of the weighting matrices. An efficient algorithm for finding the mixed sensitivity H_∞ controller is develop in this paper. The algorithm imposes the restriction

$$\left\| \vartheta M(j\omega) \right\|_\infty \leq 1 \tag{54}$$

where ϑ is a scaling factor, to be determined by the optimization process. Using the robust control toolbox command 'hinfopt' of MATLAB, we iterate ϑ until a stabilizing solution satisfying (54) is obtained. The selection of the weighing function or matrix is done with the help of the results in [26, 28]. W_1 is selected as a standard second-order weighting function [28]. The weighting functions in the form of a transfer function used in simulation are

$$\begin{aligned} W_1(s) &= \frac{2}{s^2 + s + 0.01}, \quad W_2(s) = 5, \\ W_3(s) &= \frac{100s + 1}{s + 100}. \end{aligned} \tag{55}$$

Figure 6(c) shows the variation of the singular values of the nominal, plant uncertainty and weighting functions W_1 and W_3 from low to high frequency.

Iteration 7 out of 9 gives the best answer under the tolerance of 0.0100, which has $\vartheta = 0.76563$. The order of the resulting controller is same as the order of the augmented plant, and the transfer function of the controller is

$$C(s) = \frac{\begin{array}{c} 0.23s^7 + 183.7s^6 + 2.1\cdot10^4 s^5 + 5\cdot10^5 s^4 \\ + 2.1\cdot10^6 s^3 + 3.1\cdot10^6 s^2 + 1.53\cdot10^6 s + 770.2 \end{array}}{\begin{array}{c} s^7 + 824.4s^6 + 1.15\cdot10^5 s^5 + 5.16\cdot10^6 s^4 + 1.12\cdot10^8 s^3 \\ + 1.23\cdot10^9 s^2 + 1.13\cdot10^9 s + 1.13\cdot10^7 \end{array}}. \tag{56}$$

The response of the system under specified parametric uncertainty with controller (56) is given in Fig. 15 and 16.

5.2 Kharitonov's theorem

Consider the polynomials

$$P(s) = \sum_{i=0}^{n} a_i s^i \tag{57}$$

where $\alpha_i \leq a_i \leq \beta_i$, $0 \leq i \leq n$.

According to Kharitonov's theorem, the interval polynomial $P(s)$ is stable if and only if the following four polynomials are stable [23]:

$$\begin{aligned} p_1(s) &= \alpha_0 + \alpha_1 s + \beta_2 s^2 + \beta_3 s^3 + \alpha_4 s^4 + \alpha_5 s^5 \cdots, \\ p_2(s) &= \beta_0 + \alpha_1 s + \alpha_2 s^2 + \beta_3 s^3 + \beta_4 s^4 + \alpha_5 s^5 \cdots, \\ p_3(s) &= \alpha_0 + \beta_1 s + \beta_2 s^2 + \alpha_3 s^3 + \alpha_4 s^4 + \beta_5 s^5 \cdots, \\ p_4(s) &= \beta_0 + \beta_1 s + \alpha_2 s^2 + \alpha_3 s^3 + \beta_4 s^4 + \beta_5 s^5 \cdots. \end{aligned} \tag{58}$$

In this section, the robust stability of the closed loop system is checked with proportional controllers (PC), and the stability margin of the system is also determined. The robust stability condition of the fifth order polynomials is given in [23], namely

$$\begin{aligned} &\lambda_{q3} > \lambda_{r1}, \qquad \lambda_{r3} > \max(\lambda_{q2}, \lambda_{q4}) \quad \text{and} \\ &\min(\lambda_{q2}, \lambda_{q4}) > \max(\lambda_{r2}, \lambda_{r4}) \end{aligned} \tag{59}$$

where

$$\begin{aligned} \lambda_{r1,2} &= \frac{1}{2\alpha_4}\left[\beta_2 \pm \sqrt{\beta_2^2 - 4\alpha_0\alpha_4}\right], \\ \lambda_{r3,4} &= \frac{1}{2\alpha_4}\left[\alpha_2 \pm \sqrt{\alpha_2^2 - 4\beta_0\beta_4}\right], \\ \lambda_{q1,2} &= \frac{1}{2\alpha_5}\left[\beta_3 \pm \sqrt{\beta_3^2 - 4\alpha_1\alpha_5}\right], \\ \lambda_{q3,4} &= \frac{1}{2\beta_5}\left[\alpha_3 \pm \sqrt{\alpha_3^2 - 4\beta_1\beta_5}\right]. \end{aligned}$$

The actual stability margin of the uncertain system is defined as

$$\text{Stability margin} = \min[\lambda_1, \lambda_2, \lambda_3] \tag{60}$$

where $\lambda_1 = \lambda_{q3} - \lambda_{r1}$, $\lambda_2 = \lambda_{r3} - \max(\lambda_{q2}, \lambda_{q4})$ and $\lambda_3 = \min(\lambda_{q2}, \lambda_{q4}) - \max(\lambda_{r2}, \lambda_{r4})$.

Thus, the higher the value of the stability margin, the more stable the system will be. If the stability margin is zero, the system is marginally stable; if the stability margin is negative, the system is unstable.

The transfer function of system $G(s)$ with parametric variation is given as

$$G(s) = \frac{[1.7 \times 10^7, 1.87 \times 10^8]}{\begin{array}{c} s^5 + [655,764]s^4 + [1.19\cdot10^4, 2.2\cdot10^4]s^3 \\ + [3.9\times10^4, 9.1\times10^4]s^2 + [1.56\cdot10^4, 2.5\cdot10^5]s + [5.5, 200] \end{array}}. \tag{61}$$

The characteristic equation is

$$1 + G(s) \cdot C(s) = 0. \tag{62}$$

5.3 Robust stability analysis

Case 1 Consider a simple random gain for the proportional controller (PC) to be a unit, i.e., $C(s) = 1$, hence the characteristic equation is

$$
\begin{aligned}
&s^5 + [655, 764]s^4 + \left[1.19 \cdot 10^4, 2.2 \cdot 10^4\right]s^3 \\
&\quad + \left[3.9 \times 10^4, 9.1 \times 10^4\right]s^2 \\
&\quad + \left[1.56 \cdot 10^4, 2.5 \cdot 10^5\right]s \\
&\quad + \left[1.7 \times 10^7, 1.87 \times 10^8\right] = 0. \qquad (63)
\end{aligned}
$$

Using (58) and (63), all four Kharitonov's polynomials are

$$
\begin{aligned}
p_1(s) &= s^5 + 655s^4 + 2.2 \cdot 10^4 s^3 + 9.1 \times 10^4 s^2 \\
&\quad + 1.56 \cdot 10^4 s + 1.7 \times 10^7, \\
p_2(s) &= s^5 + 764s^4 + 2.2 \cdot 10^4 s^3 + 3.9 \times 10^4 s^2 \\
&\quad + 1.56 \cdot 10^4 s + 1.87 \times 10^8, \\
p_3(s) &= s^5 + 655s^4 + 1.19 \cdot 10^4 s^3 + 9.1 \times 10^4 s^2 \\
&\quad + 2.5 \cdot 10^5 s + 1.7 \times 10^7, \\
p_4(s) &= s^5 + 764s^4 + 1.19 \cdot 10^4 s^3 + 3.9 \times 10^4 s^2 \\
&\quad + 2.5 \cdot 10^5 s + 1.87 \times 10^8. \qquad (64)
\end{aligned}
$$

By checking the stability condition (59) on (64), we see that the condition is not satisfied, hence the system is unstable.

Case 2 Consider a conventional PC with $C(s) = 0.0001$. The gain of $C(s)$ is obtained using the root locus technique which gives a value of gain of nearly 0.002 for marginal stability. Hence the characteristic equation with $C(s) = 0.0001$ is given by

$$
\begin{aligned}
&s^5 + [655, 764]s^4 + \left[1.19 \cdot 10^4, 2.2 \cdot 10^4\right]s^3 \\
&\quad + \left[3.9 \times 10^4, 9.1 \times 10^4\right]s^2 \\
&\quad + \left[1.56 \cdot 10^4, 2.5 \cdot 10^5\right]s \\
&\quad + [1705.5, 18900] = 0. \qquad (65)
\end{aligned}
$$

Using (58) and (65), we compute all four Kharitonov's polynomials, and they are

$$
\begin{aligned}
p_1(s) &= s^5 + 655s^4 + 2.2 \cdot 10^4 s^3 + 9.1 \times 10^4 s^2 \\
&\quad + 1.56 \cdot 10^4 s + 1705.5, \\
p_2(s) &= s^5 + 764s^4 + 2.2 \cdot 10^4 s^3 + 3.9 \times 10^4 s^2 \\
&\quad + 1.56 \cdot 10^4 s + 18900, \\
p_3(s) &= s^5 + 655s^4 + 1.19 \cdot 10^4 s^3 + 9.1 \times 10^4 s^2 \\
&\quad + 2.5 \cdot 10^5 s + 1705.5, \\
p_4(s) &= s^5 + 764s^4 + 1.19 \cdot 10^4 s^3 + 3.9 \times 10^4 s^2 \\
&\quad + 2.5 \cdot 10^5 s + 18900. \qquad (66)
\end{aligned}
$$

The conditions in (59) for robust stability are checked on (66) and are found to be satisfied, hence the system is stable. For the calculation of the stability margin of the system, (59), (60) and (66) are considered. From (59) and (66) the following results are obtained;

$$
\begin{aligned}
&\lambda_{r1,2} = 138.9, 0.0187, \qquad \lambda_{r3,4} = 58.97, 0.571, \\
&\lambda_{q1,2} = 2.2 \cdot 10^4, 0.71, \qquad \lambda_{q3,4} = 11879, 21,
\end{aligned}
$$

that is,

$$
\begin{aligned}
&\lambda_1 = \lambda_{q3} - \lambda_{r1} \quad \Rightarrow \quad 11879 - 138.9 = 11740.1, \\
&\lambda_2 = \lambda_{r3} - \max(\lambda_{q2}, \lambda_{q4}) \\
&\quad \Rightarrow \quad 58.97 - 21 = 37.97, \\
&\lambda_3 = \min(\lambda_{q2}, \lambda_{q4}) - \max(\lambda_{r2}, \lambda_{r4}) = 0.139.
\end{aligned}
$$

From (60), the resulting stability margin is 0.139. For a stable system, the stability margin is positive, which is true here, hence the system is stable.

Case 3 The H_∞ controller is considered as a robust PC for which the gain is derived using Routh's order reduction technique (see the Appendix). The characteristic equation with $C(s) = 6.82 \cdot 10^{-5}$ in terms of the lower and upper limit values is given as follows:

$$
\begin{aligned}
&s^5 + [655, 764]s^4 + \left[1.19 \cdot 10^4, 2.2 \cdot 10^4\right]s^3 \\
&\quad + \left[3.9 \times 10^4, 9.1 \times 10^4\right]s^2 \\
&\quad + \left[1.56 \cdot 10^4, 2.5 \cdot 10^5\right]s \\
&\quad + [1164.9, 12953] = 0. \qquad (67)
\end{aligned}
$$

After applying the stability condition given in (59) on (67), we see that the conditions are satisfied, hence the system is stable for a given uncertainty. From (59), (60) and (67), the stability margin of the system is determined, and similarly to case 2 the following results are obtained:

$$
\begin{aligned}
&\lambda_{r1,2} = 138.9, 0.0128, \qquad \lambda_{r3,4} = 59.152, 0.39, \\
&\lambda_{q1,2} = 2.2 \cdot 10^4, 0.71, \qquad \lambda_{q3,4} = 11879, 21,
\end{aligned}
$$

that is,

$$
\begin{aligned}
&\lambda_1 = \lambda_{q3} - \lambda_{r1} \quad \Rightarrow \quad 11879 - 138.9 = 11740.1, \\
&\lambda_2 = \lambda_{r3} - \max(\lambda_{q2}, \lambda_{q4}) \\
&\quad \Rightarrow \quad 59.152 - 21 = 38.152, \\
&\lambda_3 = \min(\lambda_{q2}, \lambda_{q4}) - \max(\lambda_{r2}, \lambda_{r4}) = 0.32.
\end{aligned}
$$

From (60), the resulting stability margin is 0.32. For a stable system, the stability margin is positive, which is

true in this case, hence the system is stable. The stability margin obtained from a robust PC, i.e., a PC designed using an H_∞ controller, is far better compared to the stability margin obtained from a conventional PC, i.e., a PC designed using the root locus technique.

6 Simulation results and discussion

This section presents a closed loop response for a specified vehicle speed in various modes such as acceleration, deceleration and cruise control mode for a given range of system parameters defined as lower (L), nominal (N) and upper (U) values using MATLAB and SIMULINK. These results verify the robust performance of the HEV with different controllers. Figure 7 shows the response of the throttle position of ETCS with a PI controller. In this figure, doted and solid lines represent the desired and actual values, respectively. Figure 7 shows the output of the angular throttle position in radians because the throttle position depends upon the angular movement, and hence the sinusoidal signal is taken as desired input. The throttle valve varies from 0 to $\pi/2$, i.e., from 0 to 1.57, and hence is shown between 0 to 1.5 rad.

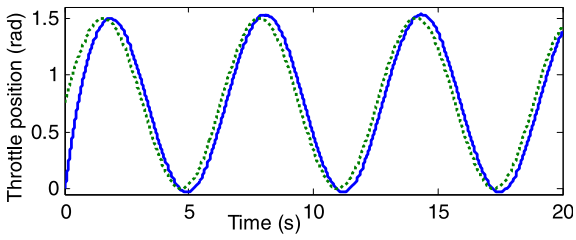

Fig. 7 Response of ETCS with PI controller

Figure 8 shows the response of the system with a PID controller in the outer loop and a PI controller in the inner loop. The response of the system with a PID and a self-tuning fuzzy PID controller is presented in Figs. 8, 9 and 10. Here the PID and PI controllers are tuned by using the hand-tuning rule [4], the values of the PID controller parameters are $K_p = 9$, $K_i = 0.1$ and $K_d = 0.3$. The integral error performance indices of these controllers under perturbation are given in Table 4. In Figs. 8–10, the vehicle speed is 20 m/s for the first 6 s, then there is an acceleration at the rate of 6 m/s^2; from then, the vehicle runs at a constant speed of 32 m/s for 8–12 s; for the time interval of 12–14 s, the vehicle runs in a decelerating mode at 4 m/s^2, reaches at the speed of 24 m/s; and finally, from 14–20 s the vehicle runs at a constant speed of 24 m/s again.

It is clear from Table 4 that the STF-PID gives a smaller value of IAE, ISE for the lower, nominal and upper values of the system parameter. Figure 10 shows the combined response of the nominal system with PID and STF-PID for comparative analysis. The performance of these two controllers in the time domain and IEPI is given in Table 5.

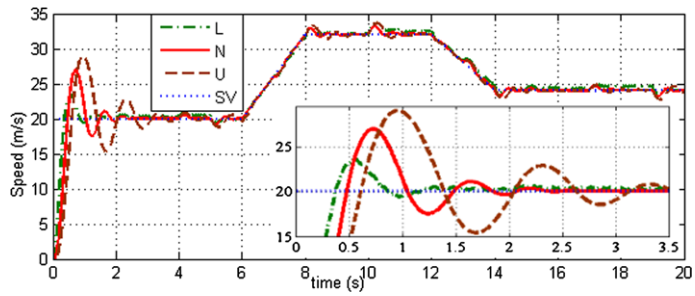

Fig. 8 Response with a PID controller

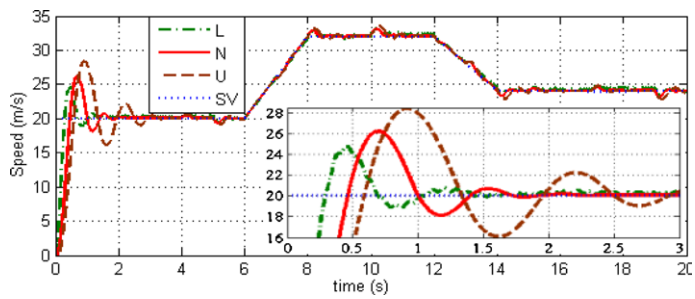

Fig. 9 Response with a self-tuning fuzzy PID controller

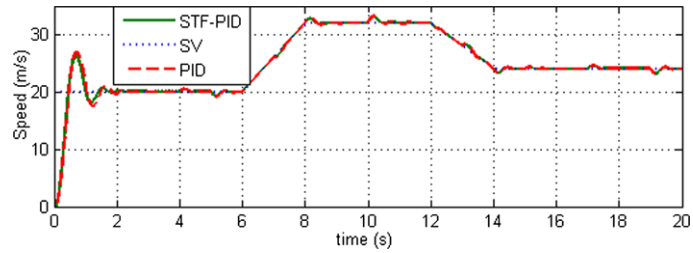

Fig. 10 Response of the nominal values of the system with PID and STF-PID

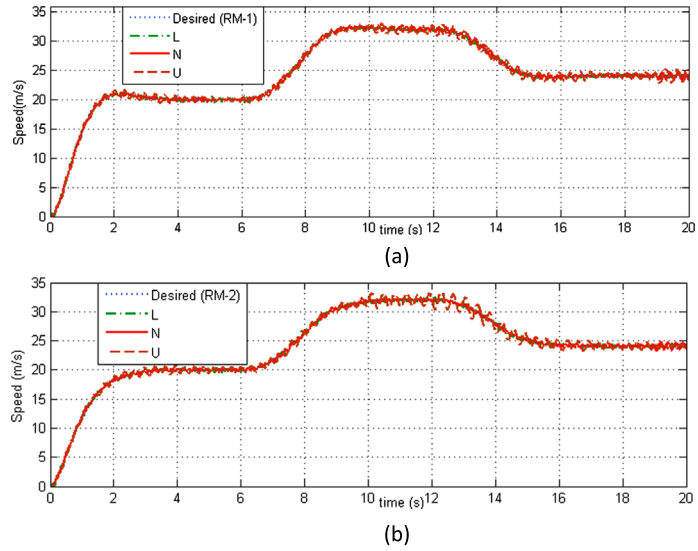

Fig. 11 Response of proposed SM-MRAS observer for (**a**) RM-1 and (**b**) RM-2

Table 4 IEPI for robustness analysis

Controller	Parameter	Lower	Nominal	Upper
PID	IAE	12.51	12.61	21.73
	ISE	69.48	114.9	179.6
STF-PID	IAE	10.66	11.33	18.89
	ISE	58.8	107.6	165

Table 5 Performance index of Controllers

Controller	IEPI		Time domain		
	IAE	ISE	OS	RT	ST
PID	12.61	114.9	34.83	0.4716	1.687
STF-PID	11.33	107.6	30.4	0.462	1.43

It is observed from Table 5 that the STF-PID controller gives better performance in the time domain as well as IEPI with respect to the PID controller.

Table 6 IEPI using SM-MRAS

Parameters		Lower	Nominal	Upper
RM-1	IAAE	3.263	4.256	9.067
	ISAE	0.7264	1.67	5.445
RM-2	IAAE	3.424	3.235	10.8
	ISAE	0.8022	0.8015	8.235

Figures 11(a)–(b) show the response of the SM-MRAS observer for RM-1 and RM-2, respectively; the observer parameters $k = 2 \cdot 10^{10}$ and $M = 0.01$ are used in the simulation.

It is clearly seen from Fig. 11(a)–(b) that the plant output tracks the desired value. It also shows the robust performance because it gives nearly the same response for a given range of system parameters. Table 6 gives the IEPI of HEV for RM-1 and RM-2, which are the values of the integral of absolute adaptation error for SM adaptation mechanisms. The integral of the absolute adaptation error (IAAE) and the integral of the

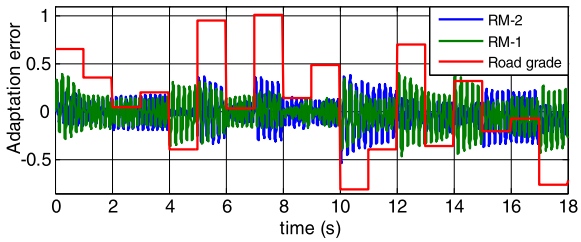

Fig. 12 Adaptation error and variation of road slope or grade

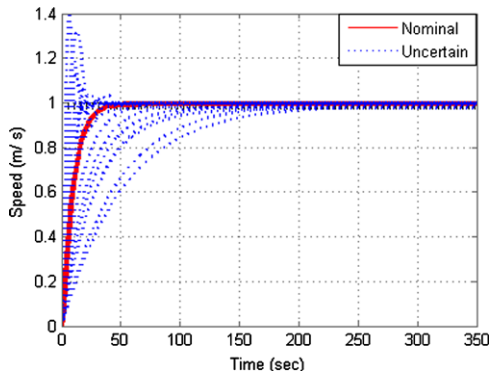

Fig. 13 Step response of the uncertain system with a conventional PC

square of the adaptation error (ISAE) are assumed to be IAE and ISE, respectively. In Fig. 11(a)–(b), the oscillations occurring in the upper plant parameters are due to chattering. For Fig. 11(a)–(b), the desired trajectory is generated from RMs 1 and 2, respectively. The input trajectory is now similar to the previous Figs. 8–10.

It is seen form Table 6 that the SM-MRAS with RM-2 gives a smaller value of IAAE and ISAE for nominal values but the SM-MRAS with RM-1 gives the least band (the difference between the upper and lower values) of IAAE and ISAE. Hence the SM-MRAS with RM-1 gives more robustness compared to RM-2. Figure 12 shows the adaptation error of MRAS with RM-1 and RM-2 and also shows the variation of road slope or grade with time which is used in all simulation results from Figs. 8 to 11.

It is clearly seen from Fig. 12 that the adaptation error depends on the road grade, i.e., for a poor road grade the adaptation error is larger.

Figures 13 and 14 respectively show the step response of HEV in the time and frequency domains (Bode plot) with a conventional PC. Figures 15 and 16 respectively show the step response of HEV in the time

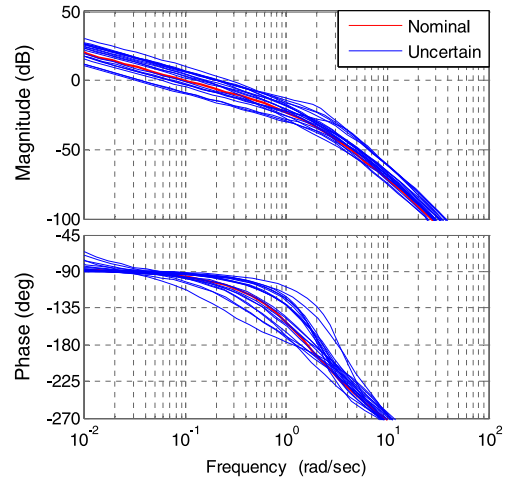

Fig. 14 Bode plot of the uncertain system with a conventional PC

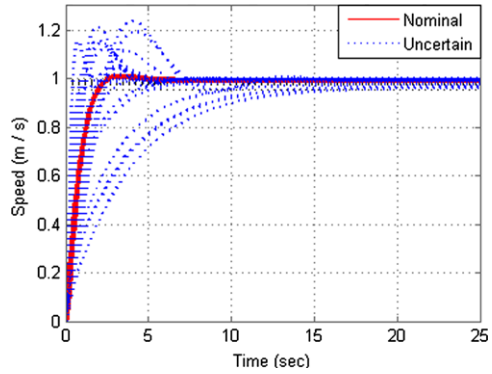

Fig. 15 Step response of the uncertain system with the H_∞ controller

and frequency domains with a robust H_∞ controller. The response in these figures is plotted after taking 20 random uncertain samples between the lower, nominal and upper limit values as given in Table 1. The performance index of the system with these controllers is given in Table 7.

From Figs. 13–16 and Table 7, it is evident that the H_∞ controller gives the smallest time domain specifications in terms of OS, ST and RT as compared to a conventional PC. Hence H_∞ gives better time domain specification as compared to conventional PC. The H_∞ controller gives the narrowest GM, PM, OS, ST and RT bands as compared to a conventional PC, meaning that narrower bands give similar performance under parameter variations, i.e., the robustness of the system towards the parametric uncertainty is achieved with the H_∞ controller.

Table 7 Performance index of uncertain system in time and frequency domain

Controller		Time domain			Frequency domain	
		OS (%)	ST (s)	RT (s)	GM (dB)	PM (deg.)
P	Nominal	2.37	35.7	19.4	29.9	83.5
	Uncertain	1.7–34.7	9.67–186	3.9–112	11.9–52.4	26.1–91.7
H_∞	Nominal	1.62	2.15	1.41	24.7	77.5
	Uncertain	0.73–26.2	1.45–12.9	0.35–9.7	13.5–34	55.3–113

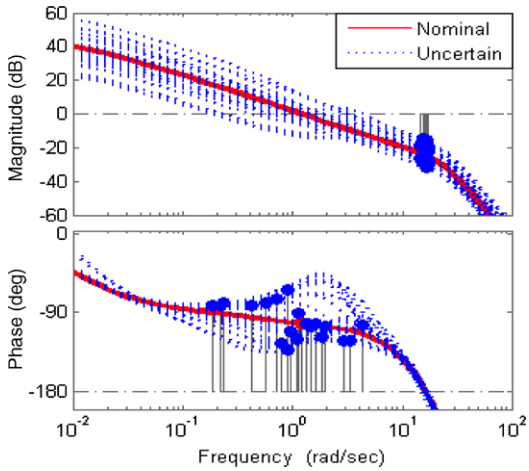

Fig. 16 Bode plot of the uncertain system with the H_∞ controller

7 Conclusion

The HEV along with ETCS is more useful for variable speed, long drives, reducing driver fatigue, improving comfort across highways and sparsely populated roads. This usually results in better fuel economy, efficiency and reduces pollution. The STF-PID controller is designed in this paper which gives robust performance and also eliminates the controller tuning time. Hence replacing the PID controller where a large time is required for tuning and robustness is also compromised. The MRAS are designed with two different RMs and nonlinear adaptation mechanisms based on the sliding mode theory for HEV. The MRAS based on the sliding mode theory is derived using Lyapunov theory to ensure asymptotic estimation stability with the advantage of fast error dynamics. A detailed comparative analysis of MRAS for estimation and control of the speed of nonlinear hybrid electrical vehicle vividly shows that the SM adaptation law with RM-1 gives better transient, steady state and robust performance as compared to MRAS with RM-2. The minimum band of IAAE and ISAE is achieved using the sliding mode adaptation mechanism with RM-1, i.e., to achieve the desired speed, a minimal change in the current and torque is required for the desired throttle position which ensures better fuel economy and efficiency. SM-MRAS may also be applied to other similar nonlinear systems for performance optimization.

The robust stability analysis of the speed control of HEV with conventional PC and robust PC is completed using robust stability condition which is derived from Kharitonov's theorem and the stability margin is also calculated. However, HEV is highly nonlinear and sensitive to parameter variation; the performance of the uncertain HEV with the robust H_∞ controller is evaluated both analytically and graphically. The robust H_∞ controller gives better performance both in the time and frequency domain. In this paper, ETCS with HEV is used in nonlinear as well as linearized form. MRAS with RM-1 is better for nonlinear HEV and the H_∞ controller is more suitable for linearized HEV. The DC servo motor used in this paper may be replaced by a brushless DC motor or a permanent magnet synchronous motor, etc.

These techniques may also be applicable for the robust stability analysis and control of PMSM, aircraft, electrical, mechanical, and electromechanical systems and other lower and higher order systems.

Appendix

The order reduction of the original seventh order H_∞ controller into a PC (zero order) using Routh's order reduction technique as given in [30, 31] is presented in this appendix. In the Routh's order reduction technique, one formulates Routh's table for the numerator and denominator of (56):

Routh's table for the numerator looks like

s^7	0.23	$2.1 \cdot 10^4$	$2.1 \cdot 10^6$	$1.53 \cdot 10^6$
s^6	183.7	$5 \cdot 10^5$	$3.1 \cdot 10^6$	770.2
s^5	$2.04 \cdot 10^4$	$2.1 \cdot 10^6$	$1.53 \cdot 10^6$	
s^4	$4.8 \cdot 10^5$	$3.1 \cdot 10^6$	770.2	
s^3	1968250	$1.53 \cdot 10^6$		
s^2	$2.73 \cdot 10^6$	770.2		
s^1	$1.53 \cdot 10^6$			
s^0	770.2			

Routh table for the denominator is

s^7	1	$1.15 \cdot 10^5$	$1.12 \cdot 10^8$	$1.13 \cdot 10^9$
s^6	824.4	$5.16 \cdot 10^6$	$1.23 \cdot 10^9$	$1.13 \cdot 10^7$
s^5	$1.09 \cdot 10^5$	$1.11 \cdot 10^8$	$1.13 \cdot 10^9$	
s^4	$4.3 \cdot 10^6$	$1.22 \cdot 10^9$	$1.13 \cdot 10^7$	
s^3	$8 \cdot 10^7$	$1.13 \cdot 10^9$		
s^2	$1.16 \cdot 10^9$	$1.13 \cdot 10^7$		
s^1	$1.13 \cdot 10^9$			
s^0	$1.13 \cdot 10^7$			

Using Routh's order reduction technique as given in [30, 31], we reduce the seventh order H_∞ controller to the second, first, and zeroth order (proportional controller); and finally, the transfer functions are respectively given below

$$\frac{2.73 \cdot 10^6 s^2 + 1.53 \cdot 10^6 s + 770.2}{1.16 \cdot 10^9 s^2 + 1.13 \cdot 10^9 s + 1.13 \cdot 10^7},$$

$$\frac{1.53 \cdot 10^6 s + 770.2}{1.13 \cdot 10^9 s + 1.13 \cdot 10^7} \quad \text{and} \quad \frac{770.2}{1.13 \cdot 10^7}.$$

The outcome of the zeroth order controller is a PC with the gain $C(s) = 6.82 \cdot 10^{-5}$. To make the calculations easy for the stability margin and robust stability analysis, consider only the reduced zeroth order H_∞ controller as a robust PC. Figure 17 shows the plots of the singular values for the nominal system with the original seventh order and reduced order, namely the second, first and zeroth order, H_∞ controllers.

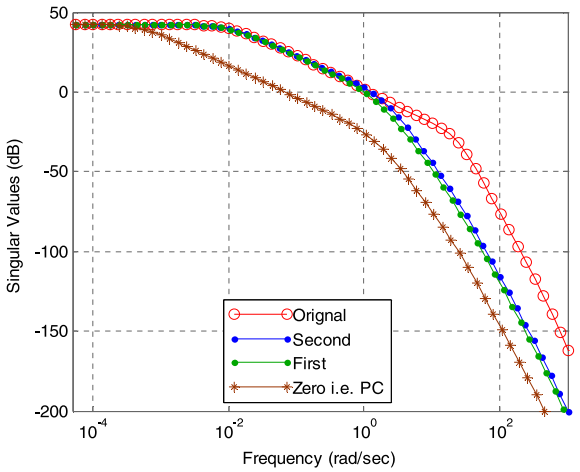

Fig. 17 Plot of the singular values for the nominal system with the original and reduced order H_∞ controllers

References

1. Husain, I.: Electric and Hybrid Vehicles, Design Fundamentals. CRC Press/Taylor and Francis, New York (2011)
2. Ehsani, M., Gao, Y., Emadi, A.: Modern Electric, Hybrid Electric and Fuel Cell Vehicles; Fundamentals, Theory and Design, 2nd edn. CRC Press/Taylor and Francis, New York (2011). First Indian reprint
3. Chau, K.T., Chan, C.C., Liu, C.: Overview of permanent magnet brushless drives for electric and hybrid electric vehicles. IEEE Trans. Ind. Electron. **55**(6) (2008)
4. Yadav, A.K., Gaur, P., Jha, S.K., Gupta, J.R.P., Mittal, A.P.: Optimal speed control of hybrid electric vehicles. J. Low Power Electron. **11**(4), 393–400 (2011)
5. Vasak, M., Baotic, M., Petrovic, I., Peric, N.: Hybrid theory-based time-optimal control of an electronic throttle. IEEE Trans. Ind. Electron. **54**(3) (2007)
6. Moura, S.J., Fathy, H.K., Callaway, D.S., Stein, J.L.: A stochastic optimal control approach for power management in plug-in hybrid electric vehicles. IEEE Trans. on Control Systems Technology **19**(3), 545–554 (2011)
7. Geng, B., Mills, J.K., Sun, D.: Energy management control of microturbine-powered plug-in hybrid electric vehicles using the telemetry equivalent consumption minimization strategy. IEEE Trans. Veh. Technol. **60**(9) (2011)
8. Borhan, H., Vahidi, A., Phillips, A.M., Kuang, M.L., Kolmanovsky, I.V., Di Cairano, S.: MPC-based energy management of a power-split hybrid electric vehicle. IEEE Transactions On Control Systems Technology **20**(3), 593–603 (2012)
9. Zhang, B., Mi, C.C., Zhang, M.: Charge-depleting control strategies and fuel optimization of blended-mode plug-in hybrid electric vehicles. IEEE Trans. Veh. Technol. **60**(4) (2011)
10. Conatsera, R., Wagnerb, J., Gantab, S., Walker, I.: Diagnosis of automotive electronic throttle control system. Control Eng. Pract. **12**, 23–30 (2004)
11. Gadoue, S.M., Giaouris, D., Finch, J.W.: MRAS sensor less vector control of an induction motor using new sliding-mode and fuzzy-logic adaptation mechanisms. IEEE Trans. Energy Convers. **25**(2) (2010)
12. Cirrincione, M., Accetta, A., Pucci, M., Vitale, G.: MRAS speed observer for high-performance linear induction motor drives based on linear neural networks. IEEE Trans. Power Electron. **28**(1), 123–134 (2013)
13. Yanga, Q., Xuea, Y., Yang, S.X., Yang, W.: An auto-tuning method for dominant-pole placement using implicit model reference adaptive control technique. J. Process Control **22**, 519–526 (2012)
14. Yang, Y., Zhou, C.: Robust adaptive fuzzy control for permanent magnet synchronous servomotor drives. Int. J. Intell. Syst. **20**, 153–171 (2005)

15. Guo, L., Parsa, L.: Model reference adaptive control of five-phase IPM motors based on neural network. IEEE Trans. Ind. Electron. **59**(3) (2012)
16. Gaur, P., Singh, B., Mittal, A.P.: Steady state and dynamic response of state space observer based PMSM drive with different controllers. J. Power Electron. **8**(3) (2008)
17. Slotine, J.J.E., Li, W.: Applied Nonlinear Control. Prentice Hall, Englewood Cliffs (1991)
18. Shin, Y.C., Xu, C.: Intelligent Systems; Modeling, Optimization, and Control. CRC Press/Taylor and Francis, New York (2009)
19. Zulfatman, Rahmat, M.F.: Application of self-tuning fuzzy PID controller on industrial hydraulic actuator using system identification approach. Int. J. Smart Sens. Intell. Syst. **2**(2) (2009)
20. Chen, Y., Wang, J.: Adaptive vehicle speed control with input injections for longitudinal motion independent road frictional condition estimation. IEEE Trans. Veh. Technol. **60**(3), 839–848 (2011)
21. An, S., Liu, W.: Robust-stability with mixed-type uncertainties. IEEE Trans. Autom. Control **49**(10) (2004)
22. Kharitonov, V.L.: Asymptotic stability of an equilibrium position of family of linear differential equation. Differ. Uravn. **14**, 2086–2088 (1978)
23. Hote, Y.V., Choudhury, D.R., Gupta, J.R.P.: Robust stability analysis PWM push–pull DC–DC converter. IEEE Trans. Power Electron. **24**(10), 2353–2356 (2009)
24. Meressi, T., Chen, D., Paden, B.: Application of Kharitonov's theorem to mechanical systems. IEEE Trans. Autom. Control **38**(3), 488–491 (1993)
25. Glover, K., Doyle, J.C.: State space formulae for all stabilizing controllers that satisfy an H_∞ norm bound and relations to risk sensitivity. Syst. Control Lett. **11**, 167–172 (1988)
26. Ortega, M.G., Rubio, F.R.: Systematic design of weighting matrices for the H_∞ mixed sensitivity problem. J. Process Control **14**, 89–98 (2004)
27. Tewari, A.: Modern Control Design with MATLAB and SIMULINK. Wiley, Chichester (2002)
28. Yang, S., Lei, Q., Peng, F.Z., Qian, Z.: A robust control scheme for grid-connected voltage-source inverters. IEEE Trans. Ind. Electron. **58**(1), 202–212 (2011)
29. Lurie, B.J., Enright, P.J.: Classical Feedback Control with MATLAB and Simulink, 2nd edn. CRC Press/Taylor and Francis, New York (2012)
30. Krishnamurthy, V., Seshadri, V.: Model reduction using the routh stability criterion. IEEE Trans. Autom. Control **23**(4), 729–731 (1978)
31. Kumar, C., Jha, S.K., Gaur, P.: Investigations of model order reduction techniques for large scale linear systems. In: Proc. of India International Conference on Power Electronics-2012 (IICPE-2012), New Delhi (2012)